Striatin-1 is a B subunit of protein phosphatase PP2A that regulates dendritic arborization and spine development in striatal neurons

Received for publication, December 19, 2017, and in revised form, May 6, 2018 Published, Papers in Press, May 25, 2018, DOI 10.1074/jbc.RA117.001519

Daniel Li, Veronica Musante, Wenliang Zhou, Marina R. Picciotto, and Angus C. Nairn[1]

From the Department of Psychiatry, Yale University, New Haven, Connecticut 06520

Edited by Roger J. Colbran

Striatin-1, a subunit of the serine/threonine phosphatase PP2A, is preferentially expressed in neurons in the striatum. As a member of the striatin family of B subunits, striatin-1 is a core component together with PP2A of a multiprotein complex called STRIPAK, the striatin-interacting phosphatase and kinase complex. Little is known about the function of striatin-1 or the STRIPAK complex in the mammalian striatum. Here, we identify a selective role for striatin-1 in striatal neuron maturation. Using a small hairpin RNA (shRNA) knockdown approach in primary striatal neuronal cultures, we determined that reduced expression of striatin-1 results in increased dendritic complexity and an increased density of dendritic spines, classified as stubby spines. The dendritic phenotype was rescued by co-expression of a striatin-1 mutant construct insensitive to the knockdown shRNA but was not rescued by co-expression of PP2A- or Mob3-binding deficient striatin-1 constructs. Reduction of striatin-1 did not result in deficits in neuronal connectivity in this knockdown model, as we observed no abnormalities in synapse formation or in spontaneous excitatory postsynaptic currents. Thus, this study suggests that striatin-1 is a regulator of neuronal development in striatal neurons.

The striatins are a highly homologous family of proteins that consist of three members: striatin-1, striatin-3/SG2NA, and striatin-4/zinedin (1, 2). Striatin proteins are ubiquitously expressed in many tissues of the body, indicative of a role in general cellular functions (3). Striatin-1 is highly expressed in medium spiny neurons in the striatum, the region of the brain in which it was first identified (1). The striatin family proteins interact with the structural (A) and catalytic (C) subunits of the protein phosphatase, PP2A, and are also termed the B‴ family of PP2A subunits (4). Within heterotrimeric PP2A complexes, striatins function as one of many regulatory B subunits thought to be responsible for substrate selection and localization of PP2A isoforms (4).

In addition to their role as B subunits of PP2A, the striatin proteins are core components of a large protein complex known as the striatin-interacting phosphatase and kinase complex (STRIPAK)[2] (5). Outside of the striatins, the core members of STRIPAK include the A and C subunits of PP2A; the members of the GCKIII kinase family, SOK1, MST3, and MST4; and the adaptor proteins CCM3, MOB3, and STRIP1 and STRIP2 (5). The STRIPAK complex also associates with a number of proteins in different signaling pathways, such as dynein (5), sarcolemmal membrane–associated protein (5), and cortactin-binding protein (6), presumably targeting them for phosphorylation and/or dephosphorylation. The diversity of the STRIPAK-associated proteins suggests a key role for STRIPAK in a range of biological systems. In addition to miscellaneous functions identified in nonmammalian organisms (7–10), STRIPAK proteins are known to coordinate cytoskeletal organization and cellular development through regulation of the actin network (11) and regulation of microtubule reorganization (12), stability (13), and morphology (12).

The various roles of PP2A in neurons have also been extensively studied. Within the striatum, PP2A is primarily known as a regulator of dopaminergic signaling through its ability to dephosphorylate DARPP-32 at several sites (14–16). The phosphorylation status of DARPP-32 has consequences for epigenetic histone modifications and memory formation (17), addiction processes (17), and striatal plasticity (18). PP2A itself is regulated by ARPP-16 (19, 20) in striatal neurons. These complex regulatory pathways allow PP2A to control key aspects of striatal signaling. Importantly, in the context of development, PP2A activity controls many elements of the cytoskeleton, including microtubules (21), actin (22), and neurofilaments (23).

Thus, as B subunits of PP2A linked to the STRIPAK complex, the striatin proteins may exert regulatory effects on a number of different signaling pathways by targeting certain proteins for dephosphorylation. Given the prevalence of striatin-1 within the striatum, these studies suggest a potential role for striatin and STRIPAK proteins in the structural organization and development of striatal neurons. In this study, we provide evidence that striatin-1 promotes neuronal maturation, more specifically by regulation of dendrite and dendritic spine growth in striatal neurons.

This work was supported by the Connecticut Mental Health Center and the State of Connecticut and by National Institutes of Health Grants DA018343, DA10044, and DA14241 from NIDA and National Institutes of Health Grant NS091336 from NINDS. The authors declare that they have no conflicts of interest with the contents of this article. The content is solely the responsibility of the authors and does not necessarily represent the official views of the National Institutes of Health.

[1] To whom correspondence should be addressed. Tel.: 203-974-7725; E-mail: angus.nairn@yale.edu.

[2] The abbreviations used are: STRIPAK, striatin-interacting phosphatase and kinase complex; shRNA, small hairpin RNA; DIV, days *in vitro*; NMJ, neuromuscular junction; EPSC, spontaneous excitatory postsynaptic current; CID, collision-induced dissociation; ANOVA, analysis of variance.

Table 1

Proteins identified by mass spectrometry analysis

Part a: Striatin-1 was immunoprecipitated from striatal tissue lysate isolated from adult mice (~6 months). Eluted proteins were identified by liquid chromatography-mass spectrometry. Score is the probability that the matched peptide is not a random event: the higher the score, the stronger the match. Expectation refers to the expectation of obtaining an equal or higher score by chance. Protein ID and Protein Name refer to the nomenclature used to identify the protein. MW is molecular weight. % coverage is the % of the protein covered by the peptide sequences. Total spectral count is a measure of the ion abundance of the species and may be used as a gross quantitative measure. Part b. Affinity purification with microcystin-Sepharose beads was performed on striatal tissue from adult rats (~6 months). Eluted proteins were separated using SDS-PAGE and gels were stained with SimplyBlue Safe Stain (Coomassie Blue). All gel bands containing prominent proteins were cut from the gel and analyzed by mass spectrometry. Headings are the same as described in Table 1a. The expectation of 0 indicates that the identity of the protein is absolutely certain.

a **Interacting Partners of Striatin-1 in Mouse Striatal Tissue**

Score	Expectation	Protein ID	Protein Name	MW	% Coverage	Total Spectral Count
988	2.9E-95	STRN_MOUSE	Striatin-1	85913	44.6	16
602	1.1E-56	CTTB2_MOUSE	Cortactin-binding protein	178662	13	11
546	3.9E-51	STRN4_MOUSE	Striatin-4 (Zinedin)	81595	27.1	12
433	8.5E-40	STRN3_MOUSE	Striatin-3 (SG2NA)	87096	24.6	9
338	2.6E-30	2AAA_MOUSE	PP2A structural subunit A	65281	27.8	10
222	1E-18	PHOCN_MOUSE	Mob3 (Phocein)	26016	56.9	6
173	8.1E-14	STRP1_MOUSE	STRIP1	95524	10	5
90	0.000019	PP2AA_MOUSE	PP2A catalytic subunit C	35585	10.4	2
20	150	PDC10_MOUSE	CCM3 (PDCD10)	24700	11.3	Tentative 1

b **Interacting Partners of PP2A A/C in Rat Striatal Tissue**

Score	Expectation	Protein ID	Protein Name	MW	% Coverage	Total Spectral Count
2206	0	STRN_RAT	Striatin-1	86173	50.5	37
1788	0	PP2AA_RAT	PP2A catalytic subunit C	35585	60.5	45
759	9.2E-73	STRN3_RAT	Striatin-3 (SG2NA)	87057	26.8	12
715	2.4E-68	2AAB_RAT	PP2A structural subunit A	65964	21.3	12
653	3.6E-62	2ABA_RAT	PP2A regulatory subunit Bα	51645	38.7	11

Results

Striatin-1 binds to members of the STRIPAK complex in mammalian striatum

Striatin family proteins have been identified as PP2A-binding partners within the STRIPAK complex in non-neuronal cell types, but little is known about the functions and targets of this complex in mammalian brain. We confirmed the assembly of the STRIPAK complex in mammalian striatum through two approaches. We first immunoprecipitated striatin-1 from striatal homogenates and identified associated proteins. We then isolated binding partners of the PP2A A/C complex in striatal homogenates using microcystin affinity purification. Microcystin is a potent inhibitor of PP1 and PP2A that has previously been used to isolate these phosphatases and their associated proteins (24). Proteins that were pulled down from these two methods were identified using MS.

Co-immunoprecipitation with striatin-1 from striatal tissue pulled down key components of the STRIPAK complex identified in previous studies, including Mob3, CCM3, and STRIP1 (Table 1, part a). Other associated proteins of interest include members of the striatin family, striatin-3 and striatin-4, the A- and C-subunits of PP2A, and CTTNBP2, an interactor of the STRIPAK complex. Of the core complex proteins identified as part of STRIPAK, only the GCKIII kinases could not be detected in the co-immunoprecipitation. Microcystin affinity purification identified striatin-1 and striatin-3 but did not pull down any other proteins that were identified in the striatin-1 co-immunoprecipitation complex (Table 1, Part b), potentially because the microcystin pulldown was analyzed only in specific gel bands. However, in the MS analysis of these proteins, the abundance of striatin-1 and striatin-3 was higher than or similar to levels of the PP2A Bα subunit, an abundant B subunit for PP2A. Thus, the striatin proteins are abundant in the striatum and are co-immunoprecipitated with the other members of the STRIPAK complex.

Striatin-1 expression levels increase with age in striatal cultures and in striatum

The expression levels of striatin-1 and its binding partners were analyzed by SDS-PAGE and immunoblotting in primary neuronal cultures taken from rat striatum or cortex at E18 (Fig. 1*a*) as well as in striatal and cortical tissue homogenates dissected from rat brain taken from birth to 6 months (Fig. 1*d*). In primary cultures, all striatin and STRIPAK proteins, including

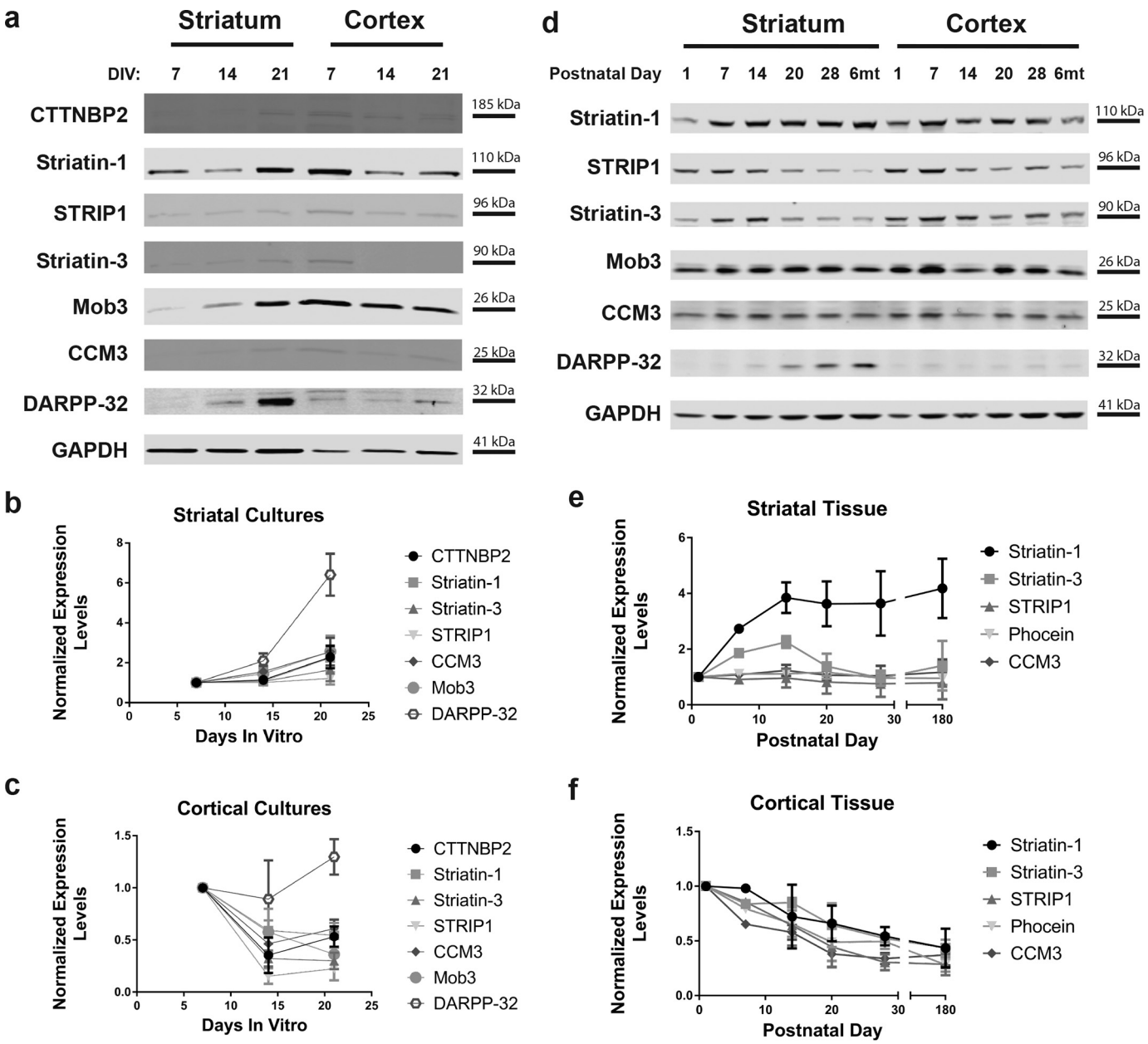

Figure 1. Expression levels of STRIPAK proteins in striatal and cortical neurons and striatal and cortical brain homogenates. *a,* primary neuronal culture was maintained for periods of 7, 14, and 21 DIV from tissue harvested from E18 rats from either striatum (*left*) or cortex (*right*). Tissue lysates were analyzed by SDS-PAGE and immunoblotting using various antibodies as indicated. DARPP-32, an abundant protein in medium spiny neurons, was used as a marker for striatal neurons. *b* and *c,* quantification of striatal (*b*) and cortical (*c*) culture immunoblots from *a*, normalized to GAPDH, $n = 3$. *d,* striatal and cortical tissue homogenates were harvested from animals through successive periods of time from P1 until adulthood (6 months; 6mt). Homogenates were analyzed by SDS-PAGE and immunoblotting using antibodies as indicated. DARPP-32 was again used as a marker for striatal neurons. *e* and *f,* quantification of striatal (*e*) and cortical (*f*) tissue immunoblots from *d*, normalized to GAPDH and to 7 DIV. $n = 1$, postnatal day 0; $n = 3$, remaining time points. All *error bars* are standard error of the mean, here and throughout.

striatin-1, striatin-3, STRIP1, CCM3, Mob3, and CTTNBP2, tended to increase in expression in striatal but not cortical cultures (Fig. 1, *b* and *c*). In contrast, there was no consistent pattern of STRIPAK protein levels by age in postnatal cortical tissue; however, in striatal tissue, the expression of striatin-1 and striatin-3 increased from P1 to P20 (Fig. 1, *e* and *f*). Thereafter, protein levels fluctuated following the P20 time point until adulthood. The increase in expression levels until P20 is consistent with the age of synaptic pruning during rodent development, as neuronal development is generally completed within the first 3 weeks of the animal's life (25). Together with the MS data, these results confirm the expression of STRIPAK complex proteins in mammalian striatal neurons. The increased expression of striatin-1 and striatin-3 during the postnatal period may suggest a potential role for STRIPAK proteins in striatal development.

Knockdown of striatin-1 results in increased dendritic outgrowth

We next investigated the potential function of striatin-1 in neuronal development by reducing its expression in cultured striatal neurons using selective small hairpin RNAs (shRNA). Two shRNA sequences targeting different regions of the

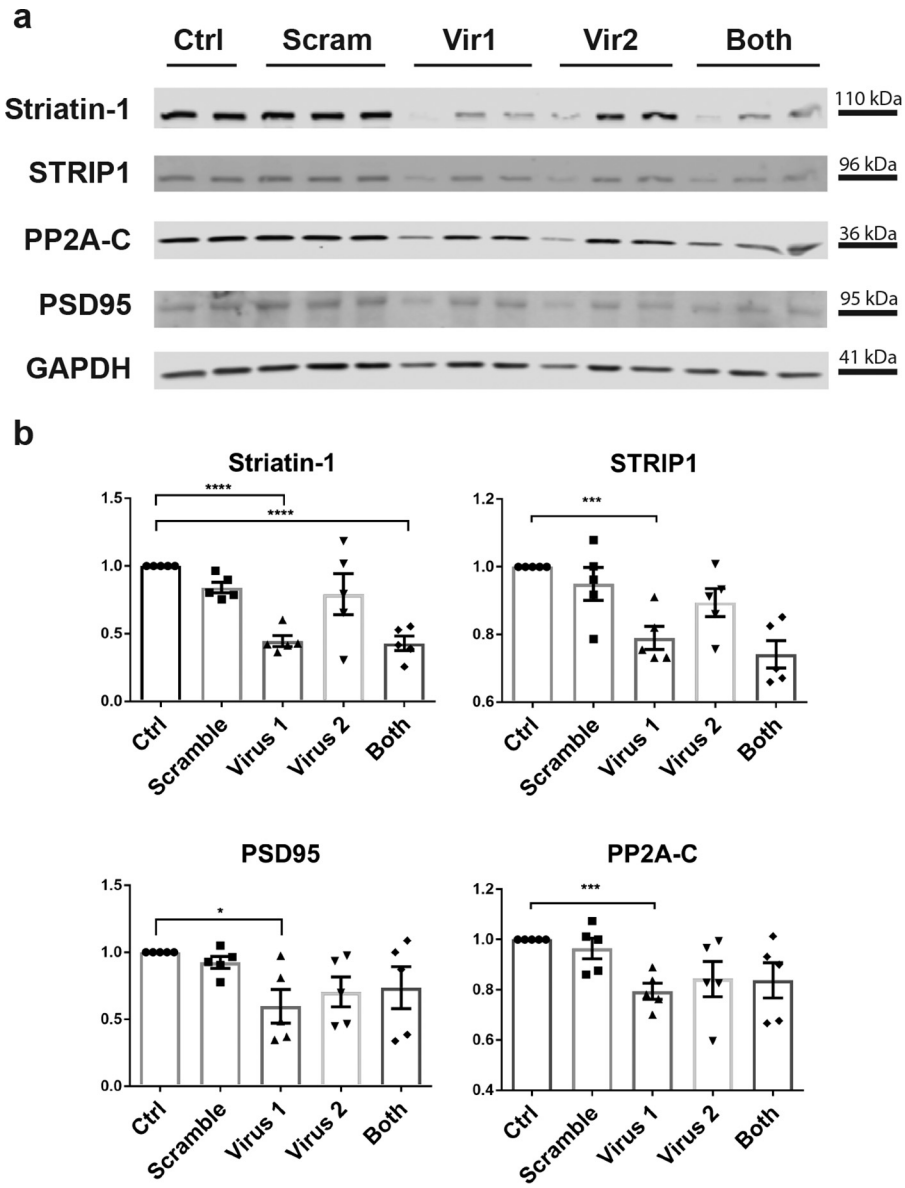

Figure 2. Validation of shRNA knockdown of striatin-1 in cultured striatal neurons. *a,* shRNA sequences were packaged into AAV2 constructs and produced using a triple-transfection, helper-free method. Two different viruses targeting different sites on striatin-1 were produced. A nonspecific scramble virus was used as a control. Primary striatal cultures derived from tissue harvested at embryonic day E18 were infected with viruses at 5DIV. Cultures were lysed at 21DIV, and samples were analyzed by immunoblotting to assess expression of striatin-1, STRIP1, PP2A-C, PSD-95, and GAPDH. *b,* quantification of the immunoblots in *a*. Expression levels of individual proteins were normalized to GAPDH, and data were analyzed using ANOVA. $n = 5$. *, $p < 0.05$; ***, $p < 0.001$; and ****, $p < 0.0001$.

mRNA were cloned into a vector and packaged into AAV2 that was used to infect primary striatal cultures cultivated from rats at E18. A scrambled shRNA sequence was also packaged into a viral construct to use as a negative control. The viruses were introduced into primary striatal cultures at 5DIV, and cells were incubated for ~2 weeks (21DIV), after which expression of striatin-1 and related STRIPAK proteins was assessed by immunoblotting (Fig. 2*a*). One of the shRNA constructs successfully reduced levels of striatin-1 (*Vir1*, Fig. 2*b*). In contrast, the scrambled sequence did not alter expression of any of the proteins examined. Interestingly, knockdown of striatin-1 also resulted in decreased expression of STRIP1 and PP2A-C, as well as the postsynaptic marker, PSD-95 (Fig. 2*b*).

We next introduced the striatin-1 shRNA into primary striatal cultures using calcium phosphate transfection. The effective shRNA sequence was cloned into a construct expressing myristoylated GFP for visualization of transfection; myristoylation facilitates the trafficking of GFP to the cell membrane and marks all compartments of the cell, including dendrites and dendritic spines (26). Neurons were fixed and immunostained with antibodies for GFP (Fig. 3, *a* and *b*). Neurons were imaged and assessed for dendritic complexity using Sholl analysis conducted both manually (Fig. 3, *c–e*) and through computer automation (Fig. 3*f*). When compared with neurons transfected with the scrambled sequence, neurons expressing striatin-1 shRNA exhibited significantly higher dendritic complexity as measured by the number of crossings at concentric circles set 50 and 100 μm from the soma (Fig. 3*e*). When the analysis was conducted using the automated Sholl analysis plugin for ImageJ (27), shRNA-expressing neurons exhibited a

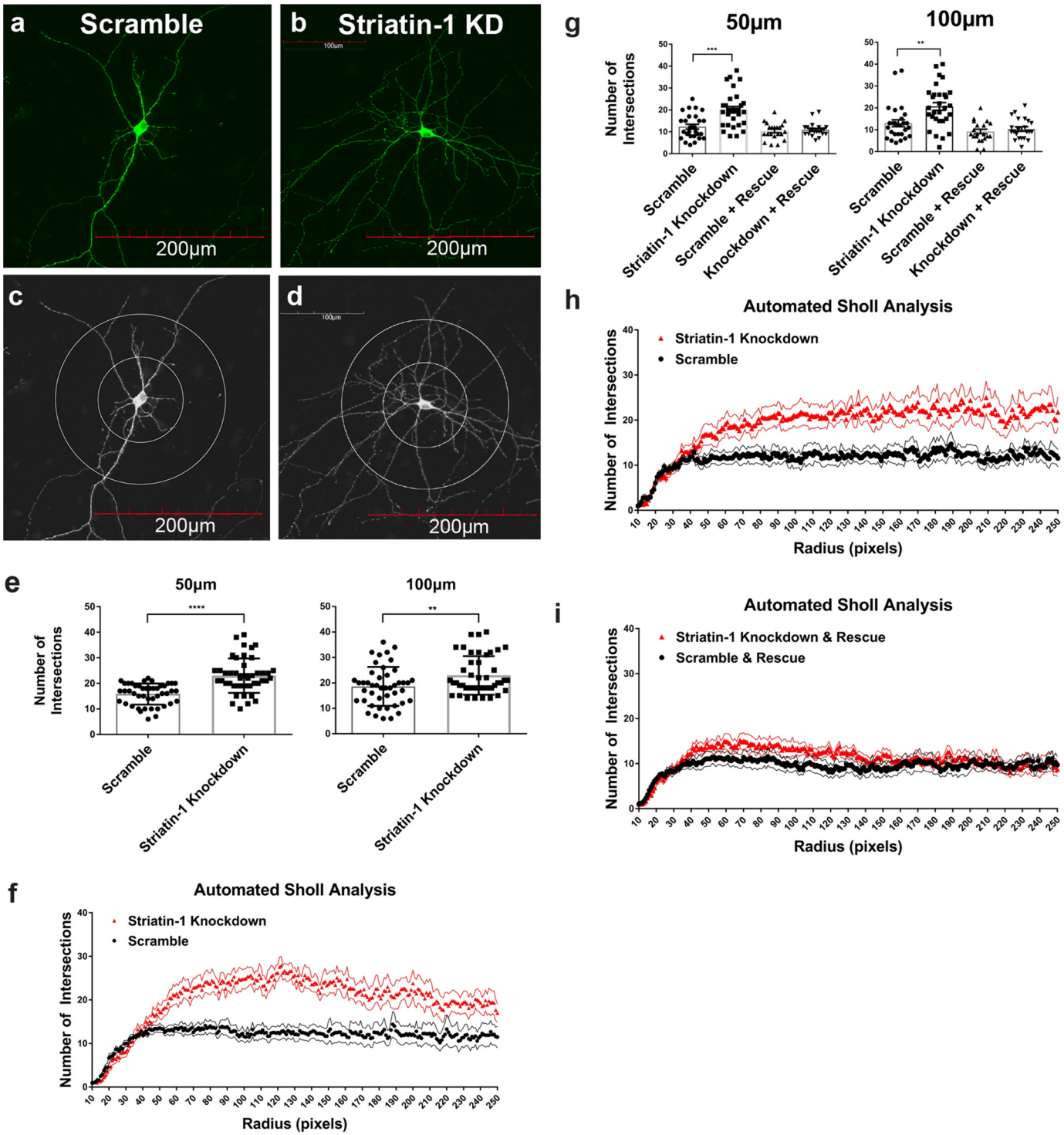

Figure 3. Knockdown of striatin-1 in striatal culture causes increased dendritic complexity. *a* and *b,* primary striatal neurons were transfected using a calcium phosphate–based method with the scramble shRNA (*a*) or the striatin-1 knockdown shRNA (*b*) packaged into a construct expressing myristoylated GFP. Transfection was used to limit the number of neurons expressing the shRNA construct. Neurons were immunostained for GFP as a marker of transfection (*green*) and imaged by confocal microscopy with a ×40 objective. *c* and *d,* scramble shRNA neurons (*c*) and the knockdown shRNA neurons (*d*) were analyzed using the Sholl method conducted manually by drawing concentric circles for each neuron at 50 and 100 μm away from the soma. The number of crossings at each concentric circle was then counted by eye. *e,* quantification of neurons transfected with either the scramble or knockdown shRNA. Data were analyzed using Student's *t* test, $n = 45$ neurons from three sets of cultures for both conditions. *f,* same neurons were analyzed using the Sholl method conducted through automation by the plug-in program "Sholl analysis" in ImageJ. The program automatically created concentric circles at each 0.1 pixel radius away from a point designated as the soma. Pixel radii equivalent for 50 and 100 μm are ~106 and 212 pixels, respectively. $n = 45$ for scramble and knockdown, the same neurons as in *e*. Upper and lower bounds show standard error of the means. *g,* neurons were transfected with the scramble shRNA alone ($n = 27$), the knockdown shRNA alone ($n = 30$), the scramble with the rescue mutant ($n = 22$), and the knockdown with the rescue mutant ($n = 22$), each from three sets of cultures. As in *e*, an effect of the knockdown was observed in neurons transfected with the knockdown shRNA alone. No effect of the knockdown shRNA was observed when co-expressed with the rescue construct. Data were analyzed using one-way ANOVA. *h* and *i,* neurons in *g* were analyzed using automated Sholl analysis as in *f*. **, $p < 0.01$; ***, $p < 0.001$; and ****, $p < 0.0001$.

higher complexity at all distances from the soma as measured in pixel radius (Fig. 3*f*).

To confirm that the excessive dendritic growth in medium spiny neurons observed was due to the decreased expression of striatin-1, we generated a striatin-1 cDNA with a mutation rendering it insensitive to shRNA binding (referred to throughout as the "rescue" construct). To ensure that expression of this construct was comparable with levels of endogenous striatin-1 in rat striatum, we analyzed equal concentrations of striatal homogenate and transfected primary striatal tissue through immunoblotting (data not shown). When quantified, the amount of striatin-1 expressed in primary striatal cultures was approximately equal to endogenous striatal striatin-1. Next, we co-transfected this rescue construct along with the striatin-1 shRNA in primary striatal cultures. As expected, the striatin-1 shRNA alone increased dendritic complexity at both 50 and 100 μm from the soma (Fig. 3*g*, *left two columns*); however, co-expression of the rescue cDNA prevented the effect of the striatin-1 shRNA (Fig. 3*g*, *right two columns*), confirming that the phenotype was specific to reduction of striatin-1 expression. These neurons were also analyzed using automated Sholl analysis (Fig. 3, *h* and *i*).

Rescue of excess dendritic growth requires intact PP2A binding

As striatin-1 is a B subunit of PP2A, we investigated whether the regulation of dendritic arborization by striatin-1 depends on PP2A. In addition, as striatin-1 and PP2A are members of the STRIPAK complex, which includes a number of other proteins, we further investigated whether striatin-1 function depended on interaction with other members of STRIPAK. To address these questions, we created PP2A-binding– deficient and Mob3-binding– deficient mutants of striatin-1 using previously validated sites (28). The PP2A-binding site is mutated at Arg-100/101, and the Mob3-binding mutant has a deletion between amino acids 230 and 344. These mutant constructs were co-transfected into primary striatal cultures with the shRNA targeting striatin-1. As before, dendritic complexity in mature neurons was measured using Sholl analysis.

PP2A- and Mob3-binding– deficient constructs did not rescue the increased dendritic complexity induced by striatin-1 knockdown, unlike the resistant construct encoding native striatin-1 (Fig. 4*a*). At both 50 and 100 μm from the soma, cells expressing either of the mutant constructs exhibited increased dendritic complexity compared with those expressing the native rescue construct. Using automated Sholl analysis (Fig. 4, *b* and *c*), there was a general trend toward increased complexity at all points throughout the dendritic arbor. These findings suggest that striatin-1 regulation of dendritic development depends on both PP2A binding and binding to Mob3, a protein present in the STRIPAK complex.

As a control for cell type in primary cultures, we ensured that all neurons examined were striatal medium spiny neurons and not cortical or glial cells. Neurons were immunostained for GFP and for DARPP-32 as a marker of medium spiny neurons (29). At 21DIV, DARPP-32 was barely detectable in primary cortical cultures (Fig. 5*a*), whereas expression was high in primary striatal cultures (Fig. 5*b*) and co-localized with GFP. The number of DARPP-32–positive cells in striatal cultures as compared with cortical cultures was measured by counting the number of positive cells per field of view (Fig. 5*c*), demonstrating that the analyzed neurons in striatal cultures were primarily medium spiny neurons.

As an additional control for cell-type–selective effects of this molecule, we investigated the effects of striatin-1 knockdown in primary cortical neurons. As in studies of striatal cultures, neurons were analyzed using the Sholl method by counting intersections at 50 and 100 μm (Fig. 5*d*) as well as through automated Sholl analysis conducted by ImageJ (Fig. 5*e*). No significant changes in dendritic complexity were observed in the cortical neurons following knockdown, indicating that striatin-1 is selectively important for maturation of medium spiny neurons.

Knockdown of striatin-1 causes an increase in density of stubby spines

We next investigated the influence of striatin-1 knockdown on the morphology of dendritic spines in striatal neurons. Dendritic spines are protrusions from the dendritic arbor that serve as synaptic contact points between neurons, generally receiving excitatory glutamatergic input (30). Dendritic spines have traditionally been categorized into three groups: stubby spines with no apparent neck; thin spines with a long neck and a small head; and mushroom spines characterized by a bulbous mushroom-shaped head (31). Spines are highly dynamic at all stages of life and rapidly turn over and transition from one state to the other (32–34). We examined the density of each type of spine in 40-μm segments of dendrites by immunostaining with GFP, comparing neurons transfected with the striatin-1 shRNA (Fig. 6*a*) with neurons transfected with the scrambled control (Fig. 6*b*). Knockdown of striatin-1 resulted in an increase in spine number per 40 μm (Fig. 6, *c*, *left two plots,* and *d*) that was due primarily to an increase in stubby spines (Fig. 6*f*). No significant difference was observed in the density of thin or mushroom spines (Fig. 6, *g* and *h*). Co-expression of the shRNA-insensitive striatin-1 cDNA prevented the effects of the shRNA, confirming the specificity of this effect (Fig. 6, *c*, *right two plots, e,* and *f*).

Striatin-1 knockdown does not impair the formation of mature synapses or functional connectivity between neurons

We next determined whether there were any changes in neuronal activity due to the increased complexity of dendrites and the density of stubby spines resulting from reduced expression of striatin-1. First, we measured the density of functional synapses following striatin-1 knockdown by immunostaining for the presynaptic vesicle protein, synapsin-1, a marker of synapses (35), and by counting the number of discrete puncta juxtaposed with GFP-labeled spines per 40 μm (Fig. 7*a*). No significant difference in the density of synapsin-1 puncta was observed between neurons transfected with the striatin-1 shRNA and neurons transfected with the scrambled control (Fig. 7*b*), indicating that the knockdown of striatin-1 does not impair the ability of mature dendritic spines to form functional connections with neighboring neurons.

We next used patch-clamp recording to assess spontaneous excitatory postsynaptic currents (EPSCs) in individual neurons following knockdown of striatin-1 in primary cultures. Sponta-

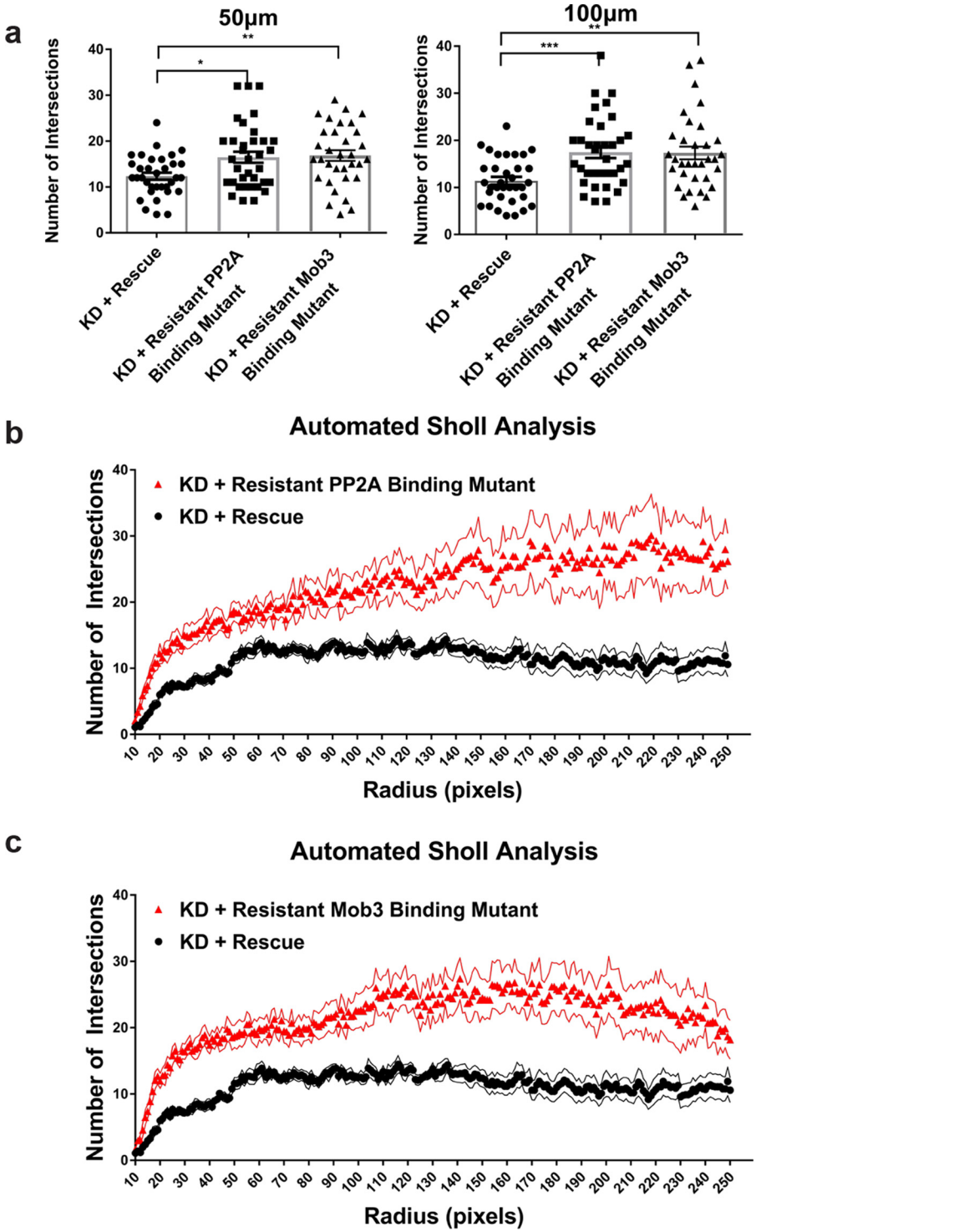

Figure 4. PP2A- and Mob3-binding mutants do not rescue increased dendritic complexity. *a,* PP2A- and Mob3-binding–deficient resistant striatin-1 mutant constructs were co-transfected with the striatin-1 knockdown shRNA. WT resistant striatin-1 was also co-transfected with the knockdown as a control. As before, neurons were analyzed by manual Sholl analysis by drawing concentric circles at 50 and 100 μm away from the soma and counting the number of intersections. Data were analyzed using one-way ANOVA; WT $n = 34$, PP2A-deficient $n = 35$, and Mob3-deficient $n = 34$, each from three sets of cultures. *b* and *c,* same neurons in *a* were also analyzed using automated Sholl analysis. Co-transfected PP2A-deficient mutant (*b*) and co-transfected Mob3-deficient mutant (*c*) are depicted separately for ease of comprehension. *, $p < 0.05$; **, $p < 0.01$; ***, $p < 0.001$.

neous EPSCs serve as a representation of functional connections on the recorded neuron, are generated in the absence of stimulation, and are driven both by presynaptic action potentials and spontaneous neurotransmitter release (36). A wide range of EPSCs was observed in control and shRNA-expressing neurons (Fig. 7, *c* and *d*), likely because individual neurons in primary culture form different numbers of connections depending on plating density, glial growth factors, and glutamatergic activation (34–38). However, this range of EPSCs was evenly distributed across both sets of conditions (Fig. 7*c*). There

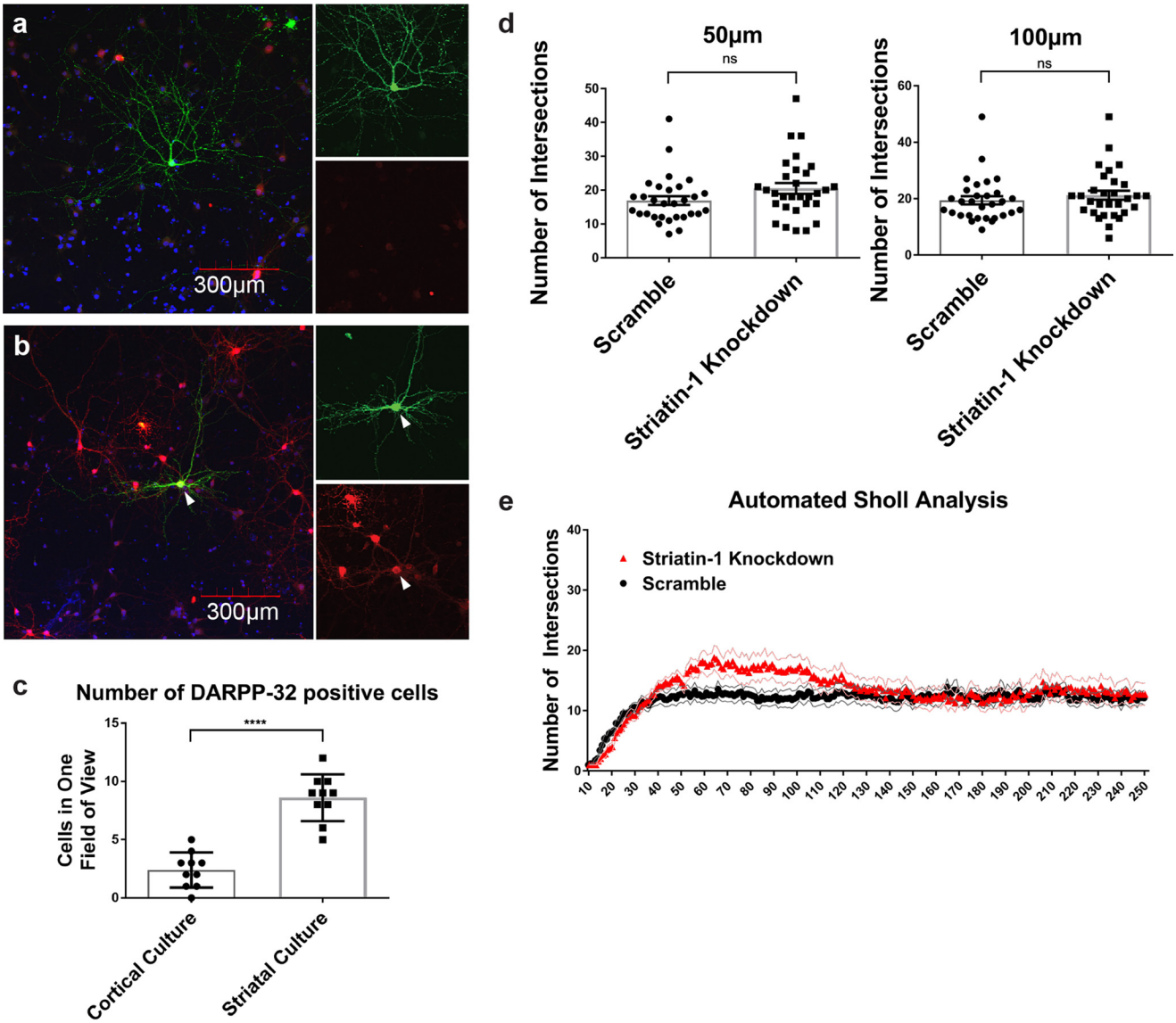

Figure 5. Striatal medium spiny neurons are identified by the marker, DARPP-32, and cortical neurons are not significantly affected by striatin-1 knockdown. *a* and *b,* preparations from cortical (*a*) and striatal (*b*) cultures were immunostained for GFP (*green*) and DARPP-32 (*red*, as a positive control for medium spiny neurons). The images display examples of neurons imaged using a ×60 objective (*left*), with cropped views of GFP and DARPP-32 on *right*. *Arrowheads* in *b* identify co-localization between GFP and DARPP-32. *c,* quantification of the number of DARPP-32–positive cells co-localizing with GFP in cultures composed primarily of cortical neurons as compared with cultures composed primarily of striatal neurons. The *y* axis shows numbers of DARPP-32–positive neurons per field of view under a ×60 objective. Data were analyzed using Student's *t* test, $n = 10$ coverslips in each condition. *d,* primary cortical neurons were transfected with scramble shRNA or striatin-1 knockdown shRNA and analyzed using the Sholl method at 50 and 100 μm away from the soma. Data were analyzed using Student's t = test, $n = 30$ neurons from three sets of cultures. *e,* same neurons were analyzed using automated Sholl analysis. *ns* is not significant. ****, $p < 0.0001$.

were no gross deficits in functional connectivity in shRNA-expressing neurons as compared with the scrambled controls (Fig. 7*d*).

Discussion

In this study, we have identified novel roles for striatin-1 in neuronal maturation and development in striatal neurons. Reduced expression of striatin-1 resulted in increased dendritic complexity that was prevented by co-expression of an shRNA-insensitive striatin-1 cDNA. Expression of mutant PP2A-binding– deficient or Mob3-binding– deficient striatin-1 constructs could not rescue this phenotype of dendritic complexity. We also observed an increase in density of dendritic spines following reduction of striatin-1, particularly in immature stubby spines, that was also prevented by expression of the rescue construct. These observations suggest that striatin-1 contributes to maturation of striatal neurons by regulating dendritic morphology, likely through its role as a binding partner of PP2A. These effects were specific to striatal neurons, as knockdown of striatin-1 in cortical neurons did not result in significant changes in dendritic morphology. This is in line with the fact that striatin-1 is predominantly expressed in the striatum. However, despite these significant changes in dendritic arborization and spine density, functional connectivity and synaptic activity in striatal neurons did not appear to be affected by knockdown of striatin-1.

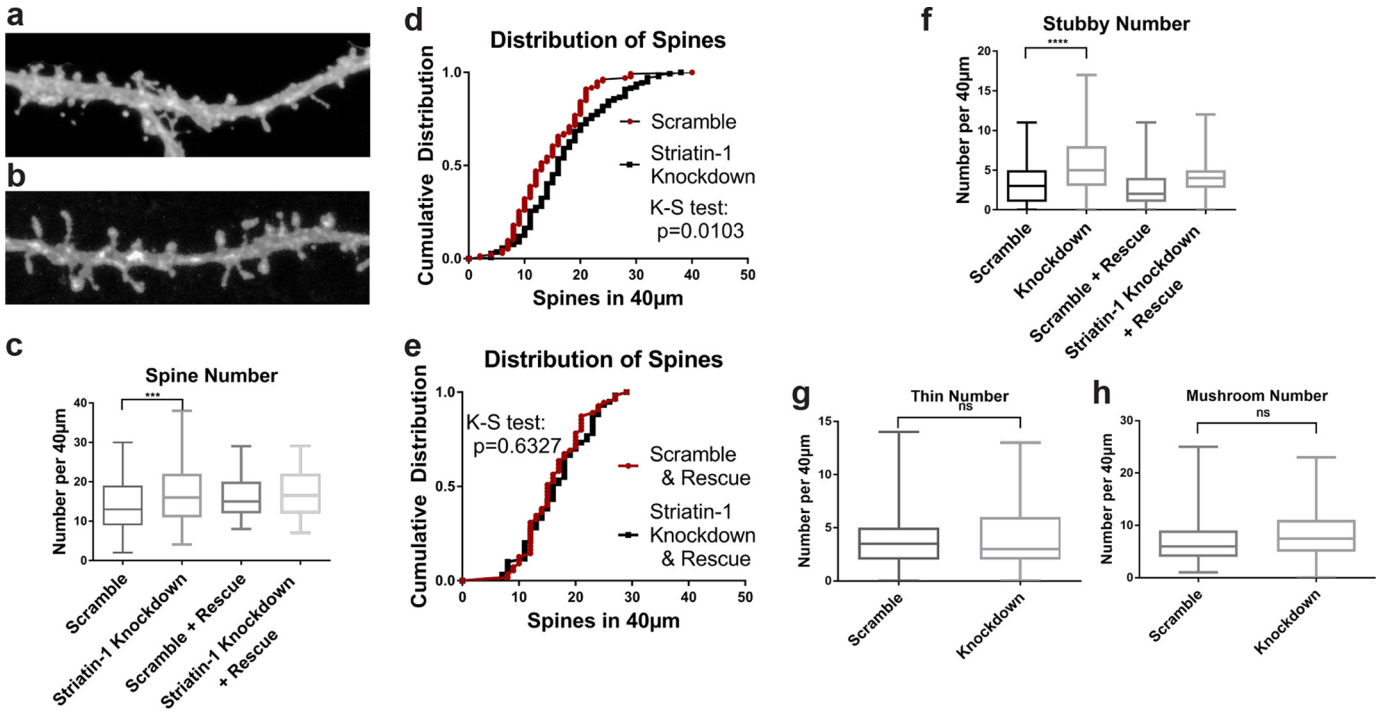

Figure 6. Reduced expression of striatin-1 causes an increased density of stubby dendritic spines. *a* and *b,* neurons were transfected using a calcium phosphate transfection method with the striatin-1 knockdown shRNA sequence (*a*) or the scramble control (*b*) packaged in a construct that allowed for co-expression of myristoylated GFP. Neurons were immunostained with GFP, and 40-μm segments of neuronal dendrites were imaged using a confocal microscope with a $\times$100 objective and a $\times$3 optical zoom. *c,* spine counting was performed using the NeuronStudio program through automated detection and classification of spine type. Data are quantified using a box and whisker plot. Scramble control shRNA: $n = 134$ dendritic segments from 35 neurons, and knockdown shRNA $n = 142$ from 36 neurons. Neurons were taken from three sets of cultures. Neurons were also co-transfected with the mutant rescue striatin-1 construct together with either the knockdown or the scramble shRNA. Scramble shRNA co-transfected with mutant, $n = 60$ from 20 neurons; knockdown shRNA co-transfected with mutant, $n = 55$ from 19 neurons. Neurons were taken from three sets of cultures. Data were analyzed using one-way ANOVA. *d,* spine data for the scramble and striatin-1 knockdown shRNAs was also quantified using a cumulative distribution analysis and assessed with the Kolmogorov-Smirnov test, a measure that provides the statistically significant difference between two cumulative distributions. The significance of the difference between the two distributions is measured at $p = 0.0103$. *e,* cumulative distribution was also plotted, and a Kolmogorov-Smirnov test was performed for neurons co-transfected with the mutant rescue striatin-1 construct together with the knockdown or the scramble shRNA. The significance is measured at $p = 0.6327$. *f–h,* stubby (*f*), thin (*g*), and mushroom (*h*) spines were analyzed using the NeuronStudio program and given an assignation based on morphology. Stubby spines had a head to neck ratio of $<$1:1. Thin spines had a head to neck ratio of $>$1:1 and a maximum head diameter of $<$0.4 μm. Mushroom spines had a head to neck ratio of $>$1:1 and a maximum head diameter of $>$0.4 μm. Data were quantified and spine density compared between scramble and knockdown neurons. All neurons were the same as in *c*: scramble shRNA, $n = 134$ from 35 neurons; knockdown shRNA, $n = 142$ from 36 neurons; scramble with mutant shRNA, $n = 60$ from 20 neurons; knockdown with mutant shRNA, $n = 55$ from 19 neurons. Data were analyzed using ANOVA (stubby) or Student's *t* test (thin, mushroom). *ns* is not significant. ***, $p < 0.001$; ****, $p < 0.0001$.

Two recent studies have also directly linked striatin and STRIPAK proteins to neuronal development. Although these studies are complementary to the data presented here, they were conducted in different cellular models and focused on synaptic development. The first study demonstrated that the STRIP1 ortholog, Strip, negatively regulated synaptic bouton development in *Drosophila* neuromuscular junctions (NMJs) by down-regulating the activity of Hippo (39), the *Drosophila* ortholog of mammalian kinases Mst1/2. It was hypothesized that Strip targeted Hippo for PP2A-dependent dephosphorylation, resulting in increased expression of an actin regulator, Ena. Additionally, knockdown of the striatin-1 *Drosophila* ortholog, cka, phenocopied the knockdown of Strip.

The second study presented evidence for striatin-4 as a regulator of dendritic spine morphology in hippocampal neurons (40). Striatin-1 and -4 share identical protein-binding domains (2), but although striatin-1 is primarily expressed in the striatum, striatin-4 is expressed throughout the central nervous system in various regions, including the hippocampus, cortex, and olfactory bulb (2). These localization differences suggest variable roles for specific striatins in different regions of the brain. Within the hippocampus, striatin-4 mRNA and protein localized to neuronal dendrites and was preferentially expressed in mushroom and stubby spines as compared with thin spines and filopodia. Stubby spines are classically viewed as immature structures as they are predominantly found during early development and are highly dynamic (34). Mushroom spines are the most developed spines, as they have large synapses and tend to persist through the lifespan of the dendrite. In this study, knockdown of striatin-4 resulted in the selective loss of mushroom spines. The authors hypothesized that striatin-4 maintained mushroom spines through its role as a scaffold for PP2A by encouraging the maturation of thin and stubby spines. Potential substrates for PP2A were not identified, but the authors suggested two known interactors of STRIPAK, CTTNBP2 (41) or the GCKIII kinases, as possible regulators of spine morphology.

The results of our study suggest that striatin-1 plays a role in both dendrite and dendritic spine regulation in striatal neurons, in contrast to the specific effect on mushroom spines observed

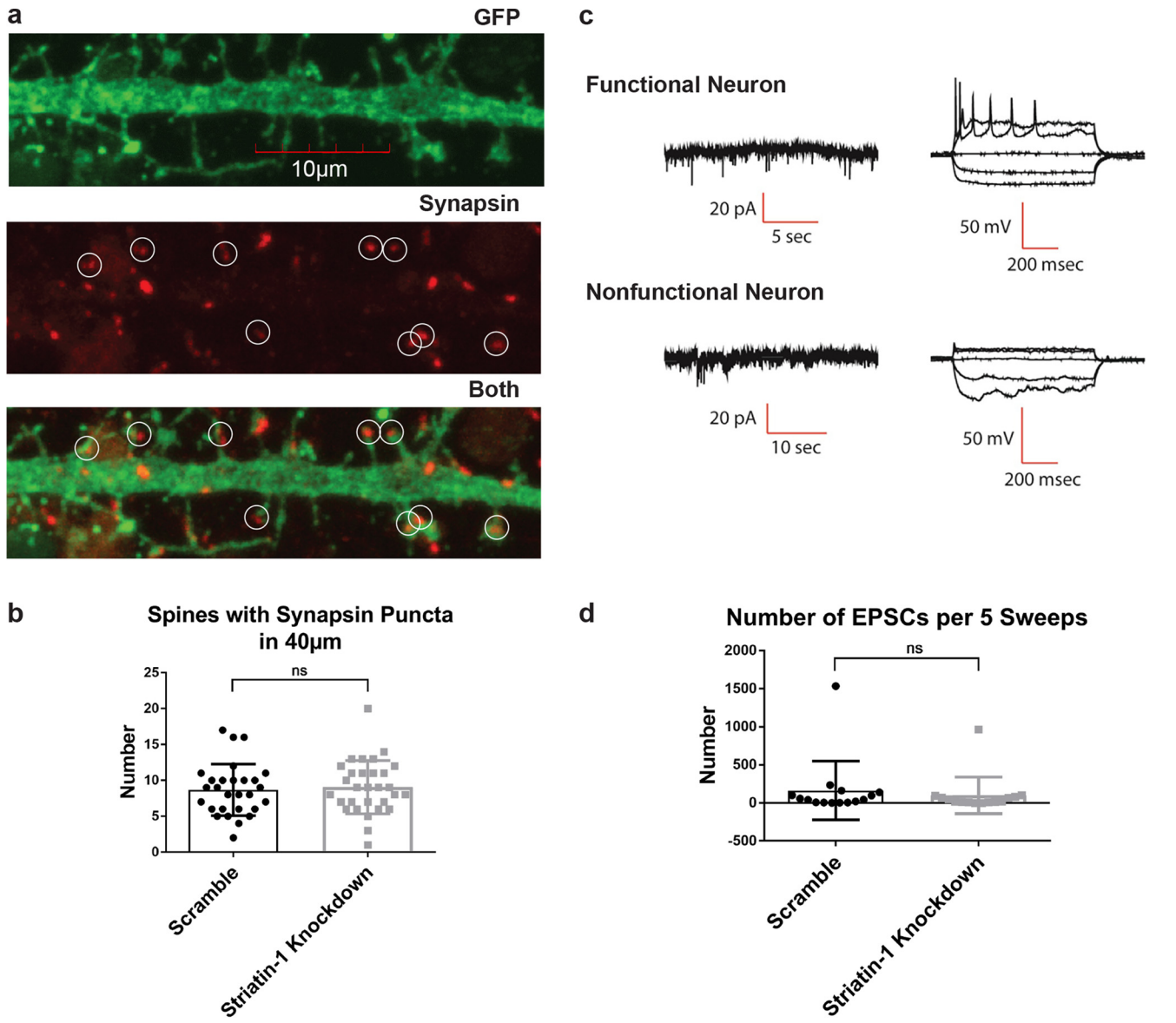

Figure 7. Knockdown of striatin-1 does not result in defects in the formation of functional synapses or connectivity between neurons. *a,* neurons were transfected with shRNA-targeting striatin-1 or a scramble shRNA, packaged within a construct that co-expressed myristoylated GFP. Antibodies were used to immunostain GFP (*green, upper panel*) and synapsin-1 (*red, middle panel*); the *lower panel* shows a merge of GFP and synapsin-1. Dendritic segments of 40 μm were imaged with a $\times$100 objective and a $\times$3 optical zoom. Synapsin-1 puncta that co-localized with a dendritic spine were counted and compared between the two conditions. *White circles* demonstrate puncta marking mature synapses in an example from a neuron that expressed the scramble shRNA. *b,* data show the number of spines with synapsin-1 puncta in dendritic segments from neurons transfected with either striatin-1 knockdown shRNA or the scramble shRNA. Scramble $n = 28$ from eight neurons, knockdown $n = 30$ from eight neurons. Data were analyzed using Student's *t* test. *c,* capability of the neurons to form functional synapses was assessed by patch-clamp electrophysiology. Neurons were transfected with the knockdown shRNA or the scramble shRNA and were GFP-positive; neurons were clamped to a constant voltage of 70 mV to record spontaneous EPSCs. Mature neurons exhibited multiple spiking patterns characteristic of EPSCs as well as induced action potentials (*upper panel*). Immature neurons did not exhibit these characteristics (*lower panel*). *d,* data show the number of EPSCs in neurons transfected with the striatin-1 knockdown shRNA or the scramble control shRNA. $n = 30$ for both conditions; neurons are from five experiments. Data were analyzed by Student's *t* test. One outlier was observed in each condition, recorded during the same experimental session, and left within the dataset as no significant difference was observed even with their removal. *ns* is not significant.

for striatin-4 in hippocampal neurons. Striatin-1 knockdown results in an increase in both dendritic complexity and stubby spine density, and these effects are specific to the striatum. Thus, striatin-1 may regulate striatal neuronal maturation by pruning unnecessary dendritic outgrowth and excessive stubby spines. Both excessive dendritic branching and stubby spine prevalence are characteristics suggestive of neuronal immaturity, indicating that these striatal neurons may be in an earlier developmental phase.

The immature dendritic phenotype observed in the striatin-1 knockdown cells was rescued by co-transfection of an shRNA-insensitive WT striatin-1 construct, but not by PP2A- and Mob3-binding–deficient constructs. Overexpression of the WT construct restored dendritic growth to baseline levels, suggesting that the levels of protein expressed were within a normal physiological range. Our data therefore identified a role for striatin-1 as a promoter of dendritic maturation that depends on its interactions with PP2A, as well as a member

of the STRIPAK complex, Mob3. It is, however, possible that the Mob3-binding mutant disrupted other functions of striatin-1 that prevented it from successful rescue, as the deletion area spanned a significant length of the construct. Nonetheless, it is suggestive that striatin-1 acts within the context of STRIPAK, binding to both PP2A and Mob3 to carry out its role.

Despite these linkages to dendritic and spine maturation, we observed no significant differences in the number of synapsin-1 puncta co-localized with dendritic spines nor in the average number of observed EPSCs in knockdown neurons in electrophysiology-based analyses. As this was a knockdown experiment, it is possible that the remaining level of striatin-1 was sufficient to establish the functional connections between the neurons in the electrophysiology experiments. If this were the case, it would be expected that complete knockout of striatin-1 would result in the loss of functional connectivity and an amplification of the increased dendritic arborization and immature spine number phenotypes observed. It is also possible that the other striatin proteins were able to compensate for the reduction in striatin-1, as levels of striatin-3 were not reduced by striatin-1 knockdown. Of note is the fact that knockdown of striatin-1 using viral expression caused a reduction in levels of STRIPAK proteins and PSD-95 despite the increase in spine number. Viral knockdown may disrupt neuronal connectivity to a greater extent than single cell transfections, resulting in greater perturbations to spine development and PSD95 expression. Alternatively, the reduction of PSD-95 could be a direct effect of striatin-1 knockdown, which would suggest that striatin-1 knockdown results in synaptic immaturity despite increasing the number of spines. Regardless, it is clear that striatin-1 plays an important role in dendritic and synaptic maturation.

As a B subunit of PP2A, striatin-1 likely exerts its physiological effects by targeting proteins for dephosphorylation. Moreover, our data indicate that disrupting striatin-1/PP2A binding impairs the ability of striatin-1 to regulate dendritic development. It will therefore be important to identify substrates of the striatin-1–PP2A complex involved in these biological phenotypes. In addition to the Mst1/Mst2 kinases implicated in the effects of Strip at the *Drosophila* NMJ, there are many potential substrates for PP2A related to neuronal development. PP2A activity has been linked to regulation of the cytoskeleton, and specifically, regulation of dendritic growth, through multiple targets (42). In a complex with the Bα subunit, PP2A binds directly to microtubules (43) as well as MAP2 (44) and τ (45), microtubule-associated phosphoproteins. MAP2 can regulate dendritic growth through microtubule (46) and actin reorganization (47, 48) and is primarily found in dendrites and dendritic spines (49). Phosphorylation of MAP2 impairs its ability to bind to microtubules (50), whereas dephosphorylation of MAP2 by PP2A results in inhibition of dendritic outgrowth (51). Although Bα has been identified as the B subunit of PP2A that binds to MAP2 and τ, striatin-1 may be an alternative B subunit in dendritic spines.

Other elements of the cytoskeleton are also regulated by PP2A. Actin plays a key role in the formation, maturation, and regulation of dendritic spines (52), and actin dynamics are primarily regulated by the Rho family of GTPases (53), including RhoA. Through its dephosphorylation of cofilin (22), a downstream target of RhoA signaling, PP2A can promote actin depolymerization (54). Actin depolymerization is linked to the loss of spine stability and the subsequent inhibition of spine head growth and plastic events (55). PP2A can also affect mitochondrial dynamics and neuronal synaptogenesis through its dephosphorylation of Drp1 (56), promoting spine development while impairing dendritic growth. Finally, PP2A dephosphorylates the neurofilament light chain (23), encouraging neurofilament assembly and axon stability (57). Neurofilaments are primarily responsible for providing axonal support and regulating axon growth and polarization of neurons (58, 59). The disruption of any of these dephosphorylation events could contribute to deficits in neuronal growth and maturation.

Experimental procedures

Antibodies and constructs

Antibodies suitable for immunoblotting were obtained as follows: striatin-1 (BD Transduction Laboratories, 610838); striatin-3/SG2NA (Abcam, ab101515); STRIP1/FAM40A (Abgent, AP9717c); Mob3/phocein (produced by Dr. Wang Min at Yale University); CCM3 (Santa Cruz Biotechnology, sc-365587); CTTNBP2 (Novus Biologicals, NBP2-32030); DARPP-32 (mouse monoclonal 6a by the Greengard Laboratory at Rockefeller University); GAPDH (EMD Millipore, CB1001-500UG); PP2A-A (Cell Signaling, 2041S); PP2A–C (Emd Millipore (05-421); and PSD-95 (Cell Signaling, 2507S). The same striatin-1 antibody was used for immunoprecipitation. For immunofluorescence, suitable antibodies were obtained for the following: rabbit GFP (Abcam, ab6556); chicken GFP (Aves, GFP1020); MAP2 (Cell Signaling, 4542S); and synapsin-1 (G246, the Greengard laboratory at Rockefeller University). Secondary antibodies for immunofluorescence were obtained from Life Technologies, Inc., including Alexa Fluor 546 goat anti-mouse (A11030), 488 goat-anti chicken (A11039), and 488 goat anti-rabbit (A11008).

For knockdown of striatin-1, we generated a construct targeting a 15-nucleotide sequence homologous across rat, mouse, and human striatin-1 (5′-TGAAGAGGCCCAATAGGTCAAAAC-3′) that was subcloned into an AAV2 vector that co-expressed GFP (provided by Dr. Ralph DiLeone at Yale University). A myristoylation sequence was cloned into the GFP expression sequence: GCCCTTCGCTCGAGACCATGGGGAGTAGCAAGAGCAAGCCTAAGGACCCCAGCCAGCGCCGGCCCGGGAGATCCACTAGTAACGGCCGCCAGTGTGCTG.

For the construct expressing striatin-1 insensitive to the shRNA knockdown, we modified a FLAG–pcDNA3–striatin-1 construct (BC090968) gifted by the Gingras lab of Mount Sinai Hospital, Toronto, Ontario, Canada. The sequence targeted by the shRNA knockdown listed above was modified to 5′-GAAGAGGCCCAACCGATCAAAAC-3′ to limit the ability of the shRNA to bind. The PP2A- and Mob3-binding–deficient mutants were modified from the previous construct using the QuikChange XL site-directed mutagenesis kit (Stratagene). For the PP2A-binding–deficient mutant, we used the forward

primer 5′-GAAAATTTGAAGAAAGATCTTGTGAGAA-GAATCAAAATGCTGGAATATGCTTTGAA-3′ and the reverse primer 5′-TTCAAAGCATATTCCAGCATTTTGATT-CTTCTCACAAGATCTTTCTTCAAATTTTC-3′. For the Mob3-binding–deficient mutant, we used the forward primer 5′-GAGGAAGACGTGGAACCCTAAGTGAACATTAAGG-AGTCACTT-3′ and the reverse primer 5′-AAGTGACTCCT-TAATGTTCACTTAGGGTTCCACGTCTTCCTC-3′. DNA sequencing identified appropriate clones.

Immunoprecipitation of striatin-1 and microcystin-Sepharose pulldown

For immunoprecipitation, tissue was collected at 6 months of age from WT C57/BL6 mice ordered from Charles River Laboratories. Brain tissue was collected and homogenized using glass/Teflon tissue homogenizers from ThermoFisher Scientific in a lysis buffer of 25 mM Tris-HCl, 150 mM NaCl, 0.1% Triton X-100, pH 8.0, with protease and phosphatase inhibitor cocktails added to a concentration of 1% (Sigma, protease inhibitor P8340; phosphatase inhibitor mixture 3 P0044). Tissue was centrifuged at 13,000 × *g* for 10 min at 4 °C, and the supernatant was collected. The supernatant was incubated with striatin-1 antibody at 4 °C for 1 h and then with protein G-Sepharose beads (Sigma, P3296) for 1 h. The beads were washed three times with 25 mM Tris-HCl, 150 mM NaCl, pH 8.0, with 0.1% Triton X-100 and then three times without Triton X-100. Protein was eluted from the Sepharose beads using 3× Laemmli buffer (made in-house) and boiling for 5 min. Proteins in pulldown samples eluted from beads were then analyzed by MS as described below.

For microcystin-Sepharose pulldown, tissue was collected from Sprague-Dawley rats (Charles River) at 6 months of age. The supernatant was incubated with microcystin-Sepharose beads (Millipore, discontinued) at 4 °C for 3 h. Beads were washed, and protein was eluted as above. For this pulldown, the protein samples were analyzed by SDS-PAGE (technique described under "Immunoblotting"). After SDS-PAGE, the gel was stained with 1× Coomassie Blue (ThermoFisher Scientific, LC6060) reagent for 2 h at room temperature and then destained with water overnight at room temperature. All visible gel bands identified by Coomassie Blue staining were cut out of the gel with a scalpel and gel bands were analyzed by MS as described below.

Mass spectrometry analysis and peptide identification

For samples eluted from beads with Laemmli buffer, a methanol/chloroform precipitation was performed. The protein pellet was resuspended in 12 μl of 8 M urea, 0.4 M NH_4HCO_3 with vigorous vortexing. Because the samples were previously reduced by the elution buffer, no further reduction was performed. Free thiols were alkylated with the addition of 3.0 μl of 100 mM iodoacetamide (Sigma, I1149) and incubation in the dark at room temperature for 20 min. The sample was diluted by adding 33 μl of water to a give a urea concentration of 2 M.

Samples were then enzymatically digested using 2 μl of 0.5 mg/ml trypsin (Promega, V5113) and incubated at 37 °C for 16 h. Digestion was halted by acidification with trifluoroacetic acid (TFA) to 0.1%. The mixtures were filtered to remove the beads and then desalted using C18 Ultra microspin columns (The Nest Group, SUM SS18V). Peptides were eluted with 2× 160 μl of 0.1% TFA, 80% acetonitrile and then dried by speed vacuum. Peptides were dissolved in 4 μl of 70% formic acid (ThermoFisher Scientific, 28905) and diluted with 20 μl of 0.1% TFA. Nanodrop measurement (ThermoFisher Scientific Nanodrop 2000 UV-visible spectrophotometer) determined the peptide concentrations (A_{260}/A_{280}). Each sample was further diluted with 0.1% TFA to 0.1 μg/μl, with 0.5 μg (5 μl) injected for LC-MS/MS analysis.

For gel bands, the bands were cut into small pieces, washed with 250 μl of 50% acetonitrile for 5 min with rocking, and then washed with 50% acetonitrile, 50 mM NH_4HCO_3 for 30 min on a tilt-table. After a final 30-min wash with 50% acetonitrile, 10 mM NH_4HCO_3, the gel pieces were dried by speed vacuum. Gel pieces were resuspended in 30 μl of 10 mM NH_4HCO_3 containing 0.20 μg of digestion grade trypsin and incubated at 37 °C for 16 h. The digestion supernatant was acidified and placed in a vial for LC-MS/MS analysis (5 μl injected).

For samples eluted from beads, LC-MS/MS analysis was performed on a ThermoFisher Scientific Orbitrap Elite equipped with a Waters nanoAcquity UPLC system utilizing a binary solvent system (Buffer A: 100% water, 0.1% formic acid; Buffer B: 100% acetonitrile, 0.1% formic acid). Trapping was performed at 5 μl/min 97% Buffer A for 3 min using a Waters Symmetry® C18 180-μm × 20-mm trap column. Peptides were separated using an ACQUITY UPLC PST (BEH) C18 nanoACQUITY column 1.7 μm, 75 μm × 250 mm (37 °C) and eluted at 300 nl/min with the following gradient: 3% Buffer B at initial conditions to 1 min; 30% B at 70 min; 50% B at 90 min; 85% B at 95–100 min; and a return to initial conditions at 101 min. MS was acquired in the Orbitrap in profile mode over the 300–2000 *m*/*z* range using 1 microscan, 30,000 resolution, AGC target of 1E6, and a full max ion time of 500 ms. Up to 15 MS/MS were collected per MS scan on species reaching an intensity threshold of 500 (charge states two and above). Data-dependent MS/MS were acquired in centroid mode in the ion trap using 1 microscan, 15,000 resolution, AGC target of 1E4, full max IT of 200 ms, 2.0 *m*/*z* isolation window, and CID fragmentation with a normalized collision energy of 35. Dynamic exclusion was enabled with a repeat count of 1, repeat duration of 30 s, exclusion list size of 500, and exclusion duration of 60 s.

For samples taken from gel pieces, trapping was performed at 5 μl/min, 99% Buffer A for 3 min using a Waters Symmetry® C18 180-μm × 20-mm trap column. Peptides were separated using an ACQUITY UPLC PST (BEH) C18 nanoACQUITY column 1.7 μm, 75 μm × 250 mm (37 °C), and eluted at 300 nl/min with the following gradient: 5% Buffer B at initial conditions to 1 min; 55% B at 50 min; 85% B at 51 min; 85% B at 55 min; and a return to initial conditions at 56 min. MS was acquired in the Orbitrap in profile mode over the 400–2000 *m*/*z* range using 1 microscan, 30,000 resolution, AGC target of 5E5, and a full max ion time of 900 ms. Up to six MS/MS were collected per MS scan on the most intense species reaching an intensity threshold of 250 (all charge states). Data-dependent MS/MS were acquired in centroid mode in the ion trap using 1 microscan, 15,000 resolution, AGC target of 1E4, full max IT of 100 ms, 2.0 *m*/*z* isolation window, and CID fragmentation with

a normalized collision energy of 35. Dynamic exclusion was enabled with a repeat count of 1, repeat duration of 30 s, exclusion list size of 500, and exclusion duration of 60 s.

To identify peptides, data were searched in-house using the Mascot algorithm (Matrix Science, version 2.4.0) for un-interpreted MS/MS spectra after using the Mascot Distiller program to generate peak lists. The data for the solution samples was searched against the SwissProt database. Search parameters used were trypsin digestion with up to 2 missed cleavages; peptide mass tolerance of 10 ppm; MS/MS fragment tolerance of 0.5 Da; variable modifications of Met oxidation and carbamidomethyl Cys. Normal and decoy database searches were searched to determine the false discovery rate, with the confidence level set to 95% ($p < 0.05$). Searches for the gel samples were similar with the follow changes: propionamide replaced carbamidomethyl as the Cys modification, and the fragment mass tolerance was set to 0.6 Da.

Preparation of brain tissue homogenates for measuring STRIPAK protein expression

All procedures were approved by the Yale University Animal Care and Use Committee (IACUC) and followed the Guide for the Care and Use of Laboratory Animals from the National Institutes of Health. WT Sprague-Dawley rats (Charles River) were sacrificed through rapid decapitation using a guillotine at postnatal days 1, 7, 14, 20, and 28, and 6 months of age. Brain tissue was lysed as described previously. Supernatant samples were denatured in 3× Laemmli buffer and boiled for 5 min in preparation for immunoblotting. A portion of the supernatant was retained to perform a BCA assay to assess the protein concentration. Samples from different time points were stored at −20 °C until the complete time course was ready.

Preparation of primary neuronal cultures

Primary cultures of striatal neurons and cortical neurons were prepared on embryonic day 18. Timed-pregnant Sprague-Dawley rats (Charles River) were sacrificed through isoflurane euthanasia. Embryos were removed from the mother through an incision in the thoracic cavity. Tissue was collected from the striatal and cortical regions of the embryos and dissociated through incubation with 0.25% trypsin for 20 min, followed by repeated trituration through glass pipettes. The resulting suspension was filtered through a 0.40-μm nylon cell strainer (Falcon, 352340). Cortical neurons were cultured as a pure cortical culture, and striatal neurons were cultured in a 60% striatal, 40% cortical mixture. A striatal/cortical mixture is necessary for proper growth and maturation of primary striatal neurons (38). Neurons were cultured on either 15-mm coverslips coated with 0.2 mg/ml poly-D-lysine or 6-well plates coated with 0.1 mg/ml poly-D-lysine. For immunofluorescence studies, including dendritic arborization and spine analysis, neurons were cultured at a density of 150,000 neurons per coverslip. For electrophysiological studies, neurons were cultured at a density of 200,000 neurons per coverslip. For verification of viral knockdown efficacy and biochemical experiments, neurons were cultured at a density of 600,000 cells per well in 6-well plates. All cultures were maintained in Neurobasal media supplemented with 2% B27, 1% Glutamax, 1% sodium pyruvate, and 0.5% penicillin/streptomycin. Media were changed for fresh media every 4–5 days.

For the study of STRIPAK protein level expression, at 7, 14, and 21 days after plating, neurons were lysed with 25 mM Tris, pH 8.0, 150 mM NaCl, 0.1% Triton X-100 with protease inhibitors at a 1% concentration. The lysate was centrifuged at 13,000 × *g* for 10 min at 4 °C, and the supernatant was collected, denatured in 3× Laemmli buffer, and boiled for 5 min in preparation for immunoblotting. A portion of the supernatant was retained to perform a BCA assay to assess the protein concentration of the sample.

Immunoblotting

Tissue homogenate and primary culture lysate samples were separated by SDS-PAGE on Novex 4–12 or 4–20% gradient gels electrophoresed at 120 V in Tris-glycine/SDS buffer. Primary culture lysate preparations were previously described. Proteins were transferred onto 0.2-μm nitrocellulose membranes in a Tris-glycine buffer with 20% methanol at 300 mA for 1.5 h. Membranes were cut to size and blocked with 5% Omniblok (nonfat dry milk in PBS and 0.1% Tween) for 1 h at room temperature and incubated with antibodies overnight at 4 °C. Antibodies were diluted in 50% PBS, 0.1% Tween and 50% Odyssey LI-COR Blocking Buffer (LI-COR P/N 927-40003) at the following concentrations: CTTNBP2 (1:500); Striatin-1 (1:1000); Striatin-3 (1:500); STRIP1 (1:1000); Mob3 (1:500); CCM3 (1:500); PP2A-A (1:1000); PP2A-C (1:2000); GAPDH (1:2000). Membranes were washed three times with PBS, 0.1% Tween and then incubated with secondary antibody, IRDye800-conjugated anti-mouse IgG (Rockland, 610-102-041) or IRDye680-conjugated anti-rabbit IgG (Bioscience, 926-6802). Blots were analyzed and quantified using an Odyssey IR Imaging System (LI-COR Bioscience, Image Studio Lite Version 5.2). Blots were processed in Image Studio Lite using default settings, and brightness was adjusted without any change in contrast. Individual images were saved as tiff files at 600 dpi. Tiff files were imported into Adobe Illustrator and figure labels added, but otherwise no changes were made to the blot images. Some antibodies (CTTNBP2, Mob3, CCM3) were detected using peroxidase-conjugated mouse secondary antibody (Vector Laboratories, PI-2000) or rabbit secondary antibody (Vector Laboratories, PI-1000) coupled with a chemiluminescence detection system (Bio-Rad ChemiDoc).

Viral production

After determination of an effective shRNA knockdown sequence as listed above and the creation of the pAAV-knockdown construct, the virus was prepared using a triple-transfection, helper-free method according to previously published protocols (60). In short, HEK293 cells grown in Dulbecco's modified Eagle's medium were transfected with pHelper (Stratagene), pRC (Stratagene), and the pAAV construct using a calcium phosphate method. A solution of 0.3 M calcium chloride mixed with the plasmids was slowly bubbled into 2× HBS and applied to the cells. Media were exchanged for fresh media after 6 h. After 72 h of incubation to allow for virus production, cells were collected and centrifuged at 1500 × *g* for 15 min and then resuspended in freezing buffer (5 M NaCl, 1 M Tris-HCl, pH 8.0).

Cells were lysed through repeated freeze-thaw cycles. Freezing was conducted in a dry ice/ethanol bath and thawing in a water bath set at 42 °C. DNA was digested using benzonase (50 units/ml) during a 30-min incubation at 37 °C. Viral supernatant was collected through centrifugation at 3700 × *g* for 20 min. The supernatant was filtered through a heparin affinity column, washed with 0.1 M NaCl, and eluted with 0.4 M NaCl. All samples and buffers were loaded through the column at a rate of 1 ml per min by hand. Elution buffer was exchanged with 1× PBS using Amicon BioMax 100,000 NMWL concentrators. The virus was subjected to a series of repeated centrifugations at 3000 × *g* for 1 h, 30 min, and 30 min to concentrate the virus. The virus was then titered and used to infect neuronal cultures that were prepared as described previously.

Neuronal culture transfections

Primary cultures of striatal neurons and cortical neurons were prepared on embryonic day 18 as described previously. Transfections were performed in neurons cultured on coverslips at 5DIV using a CalPhos mammalian transfection kit (Clontech, 631312) according to a previously published protocol for maximum efficacy of transfection (61). Briefly, media were removed from neurons and saved, and cells were incubated in fresh media. Constructs to be transfected were mixed in a calcium chloride solution at a final concentration of 0.2 M $CaCl_2$. 2× HBS, pH 7.06, was mixed with this solution, dropwise, with gentle vortexing throughout. The DNA mixture was incubated at room temperature for 15 min and then added to the cultured neurons. Cells were incubated for 1 h with the DNA mixture. Cells were then washed twice with HBS 0/2 (10 mM HEPES, 3 mM KCl, 144 mM NaCl, 2 mM $MgCl_2$). HBS 0/2 was prepared at a pH of 6.7. The original media were supplemented with 50% fresh media and added back to the cells. Cells were processed for immunofluorescence experiments 7–14 days later.

Immunofluorescence

Coverslips were prepared for immunofluorescence analysis through fixation with 4% paraformaldehyde at room temperature for 5 min. Coverslips were washed three times with PBS, 0.1% Triton and then blocked with 3% BSA, 0.1% Triton/PBS for 30 min at room temperature. Coverslips were incubated with primary antibodies for GFP, MAP2, DARPP-32, or synapsin-1 overnight at 4 °C. They were then washed twice, blocked again, and then incubated with secondary antibody for 2 h at room temperature while protected from light. Following incubation, coverslips were washed twice and mounted on glass slides using Prolong Gold with DAPI (ThermoFisher Scientific, P36931), and sealed with nail polish. The slides were imaged using confocal microscopy on an Olympus Fluoview FV1000, using the Alexa Fluor 488 and 546 dyes. For dendritic analysis, slides were imaged at ×60 with Kalman filtering applied. For spine analysis and synapsin I analysis, spines were imaged at ×100 with a ×3 zoom with Kalman filtering applied. All images were taken with 30 Z-stacks, each stack at a distance of 0.1 μm.

Dendritic arbor analysis

Manual dendritic analysis was conducted through the overlay of concentric centers in Adobe Photoshop Elements. The number of intersections across dendrites was counted manually by eye, following double-blinding of the images. The same images were then analyzed using an automated plugin created for ImageJ, Sholl Analysis. The function of the plugin allows for concentric circles to be drawn at each single pixel radius out from a point designated as the center. The number of intersections was then automatically counted. Data were plotted using GraphPad Prism software and statistical analysis performed using the tools within.

Spine analysis

Spine analysis was conducted using the NeuronStudio program. Images were uploaded into the program, and parameters were set for the automatic counting of spines. Spines were classified as stubby if the spines had a head to neck ratio of <1:1, as thin if the head to neck ratio was greater than 1:1 with a maximum head diameter of <0.4 μm, and as mushroom if the head to neck ratio was greater than 1:1 with a maximum head diameter of >0.4. Spines were automatically counted and sorted into categories; manual confirmation was performed on each individual spine that was noted by the program. Data were plotted using GraphPad Prism software and statistical analysis performed using the tools within.

Electrophysiology

The coverslips carrying the cultured cells were immersed, and all tests were performed at room temperature with oxygenated artificial cerebrospinal fluid containing (in mM): 125 NaCl, 26 $NaHCO_3$, 10 glucose, 2.3 KCl, 1.26 KH_2PO_4, 2 $CaCl_2$, and 1 $MgSO_4$, pH 7.4. Whole-cell recordings were made from visually-identified, GFP-positive neurons under voltage (V = −70 mV) clamp configuration. Electrical signals were amplified with a Multiclamp 700B and digitized with a Digidata 1440A (Molecular Devices, Sunnyvale, CA). The micropipettes were made of borosilicate glass (Warner Instruments) with a Sutter micropipette puller (P-97) and back-filled with intracellular solution containing (in mM): 135 potassium gluconate, 2 $MgCl_2$, 10 Na_2 phosphocreatine, 3 Na_2ATP, 0.3 Na_2GTP, and 10 HEPES, pH 7.3.

Electrophysiology data analysis

Electrical recording data of evoked currents were analyzed using Clampfit 10 (Molecular Devices, Sunnyvale, CA). Traces were filtered with Gaussian low-pass with 500 Hz cutoff before current amplitude measurements. Miniature EPSCs were analyzed using Axograph ×1.5.5 (Axograph Scientific, Berkeley, CA), as described previously (26). Briefly, traces were filtered with Gaussian low-pass with 500 Hz cutoff before event searching. A template EPSC was defined with amplitude −20 pA, rise 0.5 ms, and decay 3 ms, and only those EPSCs with amplitude >= −10 pA were counted. Following programmed event detection, all events were examined by eye to be counted as EPSCs. All statistics were done on raw data. Unpaired Student's *t* tests were used for determining statistical difference. Values are pre-

sented as mean ± S.E. Statistical analysis was performed by Student's *t* test followed by Tukey post hoc test. Statistical significance was defined as $p < 0.05$.

Author contributions—D. L., V. M., and A. C. N. conceptualization; D. L., V. M., and W.-L. Z. data curation; D. L. validation; D. L., V. M., W.-L. Z., and A. C. N. methodology; D. L. and A. C. N. writing-original draft; D. L. project administration; D. L., V. M., W.-L. Z., M. R. P., and A. C. N. writing-review and editing; V. M., M. R. P., and A. C. N. supervision; M. R. P. and A. C. N. funding acquisition; A. C. N. resources.

Acknowledgments—We thank Becky Carlyle and Rivka Schwarcz for their assistance with experimental procedures, Rashaun Wilson for help in data analysis, and Darren Wilson and Rich Trinko for assistance in virus production. We thank Drs. Sreeganga Chandra, Anthony Koleske, and Paul Lombroso for guidance. We thank Drs. Wang Min, Anne-Claude Gingras, and Paul Greengard for constructs and antibodies. We also thank Dr. Jean Kanyo of the Yale/NIDA Neuroproteomics Center for proteomics analysis. Electrophysiology work was supported by National Institutes of Health Grant DA14241. Proteomics analysis was supported by Yale/National Institutes of Health Neuroproteomics Center Grant DA018343 from NIDA.

References

1. Benoist, M., Gaillard, S., and Castets, F. (2006) The striatin family: a new signaling platform in dendritic spines. *J. Physiol.* **99,** 146–153 Medline
2. Castets, F., Rakitina, T., Gaillard, S., Moqrich, A., Mattei, M. G., and Monneron, A. (2000) Zinedin, SG2NA, and striatin are calmodulin-binding, WD repeat proteins principally expressed in the brain. *J. Biol. Chem.* **275,** 19970–19977 CrossRef Medline
3. Hwang, J., and Pallas, D. C. (2014) STRIPAK complexes: structure, biological function, and involvement in human diseases. *Int. J. Biochem. Cell Biol.* **47,** 118–148 CrossRef Medline
4. Moreno, C. S., Park, S., Nelson, K., Ashby, D., Hubalek, F., Lane, W. S., and Pallas, D. C. (2000) WD40 repeat proteins striatin and S/G(2) nuclear autoantigen are members of a novel family of calmodulin-binding proteins that associate with protein phosphatase 2A. *J. Biol. Chem.* **275,** 5257–5263 CrossRef Medline
5. Goudreault, M., D'Ambrosio, L. M., Kean, M. J., Mullin, M. J., Larsen, B. G., Sanchez, A., Chaudhry, S., Chen, G. I., Sicheri, F., Nesvizhskii, A. I., Aebersold, R., Raught, B., and Gingras, A.-C. (2009) A PP2A phosphatase high density interaction network identifies a novel striatin-interacting phosphatase and kinase complex linked to the cerebral cavernous malformation 3 (CCM3) protein. *Mol. Cell. Proteomics* **8,** 157–171 CrossRef Medline
6. Gaillard, S., Bartoli, M., Castets, F., and Monneron, A. (2001) Striatin, a calmodulin-dependent scaffolding protein, directly binds caveolin-1. *FEBS Lett.* **508,** 49–52 CrossRef Medline
7. Xiang, Q., Rasmussen, C., and Glass, N. L. (2002) The ham-2 locus, encoding a putative transmembrane protein, is required for hyphal fusion in *Neurospora crassa*. *Genetics* **160,** 169–180 Medline
8. Baryshnikova, A., Costanzo, M., Kim, Y., Ding, H., Koh, J., Toufighi, K., Youn, J.-Y., Ou, J., San Luis, B.-J., Bandyopadhyay, S., Hibbs, M., Hess, D., Gingras, A.-C., Bader, G. D., Troyanskaya, O. G., *et al.* (2010) Quantitative analysis of fitness and genetic interactions in yeast on a genome scale. *Nat. Methods* **7,** 1017–1024 CrossRef Medline
9. Chen, H.-W., Marinissen, M. J., Oh, S.-W., Chen, X., Melnick, M., Perrimon, N., Gutkind, J. S., and Hou, S. X. (2002) CKA, a novel multidomain protein, regulates the JUN N-terminal kinase signal transduction pathway in *Drosophila*. *Mol. Cell. Biol.* **22,** 1792–1803 CrossRef Medline
10. Friedman, A., and Perrimon, N. (2006) A functional RNAi screen for regulators of receptor tyrosine kinase and ERK signalling. *Nature* **444,** 230–234 CrossRef Medline
11. Bai, S., Herrera-Abreu, M. T., Rohn, J. L., Racine, V., Tajadura, V., Suryavanshi, N., Bechtel, S., Wiemann, S., Baum, B., and Ridley, A. J. (2011) Identification and characterization of a set of conserved and new regulators of cytoskeletal organization, cell morphology and migration. *BMC Biol.* **9,** 54 CrossRef Medline
12. Schulte, J., Sepp, K. J., Jorquera, R. A., Wu, C., Song, Y., Hong, P., and Littleton, J. T. (2010) DMob4/Phocein regulates synapse formation, axonal transport, and microtubule organization. *J. Neurosci.* **30,** 5189–5203 CrossRef Medline
13. Sakuma, C., Okumura, M., Umehara, T., Miura, M., and Chihara, T. (2015) A STRIPAK component Strip regulates neuronal morphogenesis by affecting microtubule stability. *Sci. Rep.* **5,** 17769 Medline
14. Ahn, J.-H., Sung, J. Y., McAvoy, T., Nishi, A., Janssens, V., Goris, J., Greengard, P., and Nairn, A. C. (2007) The B″/PR72 subunit mediates Ca^{2+}-dependent dephosphorylation of DARPP-32 by protein phosphatase 2A. *Proc. Natl. Acad. Sci. U.S.A.* **104,** 9876–9881 CrossRef Medline
15. Nishi, A., Bibb, J. A., Matsuyama, S., Hamada, M., Higashi, H., Nairn, A. C., and Greengard, P. (2002) Regulation of DARPP-32 dephosphorylation at PKA- and Cdk5-sites by NMDA and AMPA receptors: distinct roles of calcineurin and protein phosphatase-2A. *J. Neurochem.* **81,** 832–841 CrossRef Medline
16. Nishi, A., Matamales, M., Musante, V., Valjent, E., Kuroiwa, M., Kitahara, Y., Rebholz, H., Greengard, P., Girault, J. A., and Nairn, A. C. (2017) Glutamate counteracts dopamine/pka signaling via dephosphorylation of DARPP-32 Ser-97 and alteration of its cytonuclear distribution. *J. Biol. Chem.* **292,** 1462–1476 CrossRef Medline
17. Stipanovich, A., Valjent, E., Matamales, M., Nishi, A., Ahn, J.-H., Maroteaux, M., Bertran-Gonzalez, J., Brami-Cherrier, K., Enslen, H., Corbillé, A.-G., Filhol, O., Nairn, A. C., Greengard, P., Hervé, D., and Girault, J.-A. (2008) A phosphatase cascade by which rewarding stimuli control nucleosomal response. *Nature* **453,** 879–884 CrossRef Medline
18. Calabresi, P., Gubellini, P., Centonze, D., Picconi, B., Bernardi, G., Chergui, K., Svenningsson, P., Fienberg, A. A., and Greengard, P. (2000) Dopamine and cAMP-regulated phosphoprotein 32 kDa controls both striatal long-term depression and long-term potentiation, opposing forms of synaptic plasticity. *J. Neurosci.* **20,** 8443–8451 CrossRef Medline
19. Musante, V., Li, L., Kanyo, J., Lam, T. T., Colangelo, C. M., Cheng, S. K., Brody, A. H., Greengard, P., Le Novère, N., and Nairn, A. C. (2017) Reciprocal regulation of ARPP-16 by PKA and MAST3 kinases provides a cAMP-regulated switch in protein phosphatase 2A inhibition. *Elife* **6,** e24998 Medline
20. Andrade, E. C., Musante, V., Horiuchi, A., Matsuzaki, H., Brody, A. H., Wu, T., Greengard, P., Taylor, J. R., and Nairn, A. C. (2017) ARPP-16 is a striatal-enriched inhibitor of protein phosphatase 2A regulated by microtubule-associated serine/threonine kinase 3 (Mast 3 kinase). *J. Neurosci.* **37,** 2709–2722 CrossRef Medline
21. Hiraga, A., and Tamura, S. (2000) Protein phosphatase 2A is associated in an inactive state with microtubules through 2A1-specific interaction with tubulin. *Biochem. J.* **346,** 433–439 CrossRef Medline
22. Ambach, A., Saunus, J., Konstandin, M., Wesselborg, S., Meuer, S. C., and Samstag, Y. (2000) The serine phosphatases PP1 and PP2A associate with and activate the actin-binding protein cofilin in human T lymphocytes. *Eur. J. Immunol.* **30,** 3422–3431 CrossRef Medline
23. Saito, T., Shima, H., Osawa, Y., Nagao, M., Hemmings, B. A., Kishimoto, T., and Hisanaga, S. (1995) Neurofilament-associated protein phosphatase 2A: its possible role in preserving neurofilaments in filamentous states. *Biochemistry* **34,** 7376–7384 CrossRef Medline
24. MacKintosh, C., Beattie, K. A., Klumpp, S., Cohen, P., and Codd, G. A. (1990) Cyanobacterial microcystin-LR is a potent and specific inhibitor of protein phosphatases 1 and 2A from both mammals and higher plants. *FEBS Lett.* **264,** 187–192 CrossRef Medline
25. Semple, B. D., Blomgren, K., Gimlin, K., Ferriero, D. M., and Noble-Haeusslein, L. J. (2013) Brain development in rodents and humans: identifying benchmarks of maturation and vulnerability to injury across species. *Prog. Neurobiol.* **106,** 1–16 Medline
26. Kameda, H., Furuta, T., Matsuda, W., Ohira, K., Nakamura, K., Hioki, H., and Kaneko, T. (2008) Targeting green fluorescent protein to dendritic membrane in central neurons. *Neurosci. Res.* **61,** 79–91 CrossRef Medline

27. Ferreira, T. A., Blackman, A. V., Oyrer, J., Jayabal, S., Chung, A. J., Watt, A. J., Sjöström, P. J., and van Meyel, D. J. (2014) Neuronal morphometry directly from bitmap images. *Nat. Methods* **11,** 982–984 CrossRef Medline
28. Gordon, J., Hwang, J., Carrier, K. J., Jones, C. A., Kern, Q. L., Moreno, C. S., Karas, R. H., and Pallas, D. C. (2011) Protein phosphatase 2a (PP2A) binds within the oligomerization domain of striatin and regulates the phosphorylation and activation of the mammalian Ste20-Like kinase Mst3. *BMC Biochem.* **12,** 54 CrossRef Medline
29. Matamales, M., Bertran-Gonzalez, J., Salomon, L., Degos, B., Deniau, J.-M., Valjent, E., Hervé, D., and Girault, J.-A. (2009) Striatal medium-sized spiny neurons: identification by nuclear staining and study of neuronal subpopulations in BAC transgenic mice. *PLoS ONE* **4,** e4770 CrossRef Medline
30. Hering, H., and Sheng, M. (2001) Dendritic spines: structure, dynamics and regulation. *Nat. Rev. Neurosci.* **2,** 880–888 CrossRef Medline
31. Yuste, R., and Bonhoeffer, T. (2004) Genesis of dendritic spines: insights from ultrastructural and imaging studies. *Nat. Rev. Neurosci.* **5,** 24–34 CrossRef Medline
32. Nimchinsky, E. A., Sabatini, B. L., and Svoboda, K. (2002) Structure and function of dendritic spines. *Annu. Rev. Physiol.* **64,** 313–353 CrossRef Medline
33. Bourne, J., and Harris, K. M. (2007) Do thin spines learn to be mushroom spines that remember? *Curr. Opin. Neurobiol.* **17,** 381–386 CrossRef Medline
34. Berry, K. P., and Nedivi, E. (2017) Spine dynamics: are they all the same? *Neuron* **96,** 43–55 CrossRef Medline
35. Thiel, G. (1993) Synapsin I, synapsin II, and synaptophysin: marker proteins of synaptic vesicles. *Brain Pathol.* **3,** 87–95 CrossRef Medline
36. Pinheiro, P. S., and Mulle, C. (2008) Presynaptic glutamate receptors: physiological functions and mechanisms of action. *Nat. Rev. Neurosci.* **9,** 423–436 CrossRef Medline
37. Falk, T., Zhang, S., Erbe, E. L., and Sherman, S. J. (2006) Neurochemical and electrophysiological characteristics of rat striatal neurons in primary culture. *J. Comp. Neurol.* **494,** 275–289 CrossRef Medline
38. Penrod, R. D., Kourrich, S., Kearney, E., Thomas, M. J., and Lanier, L. M. (2011) An embryonic culture system for the investigation of striatal medium spiny neuron dendritic spine development and plasticity. *J. Neurosci. Methods* **200,** 1–13 CrossRef Medline
39. Sakuma, C., Saito, Y., Umehara, T., Kamimura, K., Maeda, N., Mosca, T. J., Miura, M., and Chihara, T. (2016) The strip-hippo pathway regulates synaptic terminal formation by modulating actin organization at the *Drosophila* neuromuscular synapses. *Cell Rep.* **16,** 2289–2297 CrossRef Medline
40. Lin, L., Lo, L. H., Lyu, Q., and Lai, K.-O. (2017) Determination of dendritic spine morphology by the striatin scaffold protein STRN4 through interaction with the phosphatase PP2A. *J. Biol. Chem.* **292,** 9451–9464 CrossRef Medline
41. Chen, Y.-K., Chen, C.-Y., Hu, H.-T., and Hsueh, Y.-P. (2012) CTTNBP2, but not CTTNBP2NL, regulates dendritic spinogenesis and synaptic distribution of the striatin-PP2A complex. *Mol. Biol. Cell.* **23,** 4383–4392 CrossRef Medline
42. Hoffman, A., Taleski, G., and Sontag, E. (2017) The protein serine/threonine phosphatases PP2A, PP1, and calcineurin: a triple threat in the regulation of the neuronal cytoskeleton. *Mol. Cell. Neurosci.* **84,** 119–131 CrossRef Medline
43. Sontag, E., Nunbhakdi-Craig, V., Bloom, G. S., and Mumby, M. C. (1995) A novel pool of protein phosphatase 2A is associated with microtubules and is regulated during the cell cycle. *J. Cell Biol.* **128,** 1131–1144 CrossRef Medline
44. Sánchez, C., Díaz-Nido, J., and Avila, J. (2000) Phosphorylation of microtubule-associated protein 2 (MAP2) and its relevance for the regulation of the neuronal cytoskeleton function. *Prog. Neurobiol.* **61,** 133–168 CrossRef Medline
45. Martin, L., Latypova, X., Wilson, C. M., Magnaudeix, A., Perrin, M. L., Yardin, C., and Terro, F. (2013) Tau protein kinases: Involvement in Alzheimer's disease. *Ageing Res. Rev.* **12,** 289–309 CrossRef Medline
46. Gamblin, T. C., Nachmanoff, K., Halpain, S., and Williams, R. C. (1996) Recombinant microtubule-associated protein 2c reduces the dynamic instability of individual microtubules. *Biochemistry* **35,** 12576–12586 CrossRef Medline
47. Farah, C. A., and Leclerc, N. (2008) HMWMAP2: new perspectives on a pathway to dendritic identity. *Cell Motil. Cytoskeleton* **65,** 515–527 CrossRef Medline
48. Roger, B., Al-Bassam, J., Dehmelt, L., Milligan, R. A., and Halpain, S. (2004) MAP2c, but not tau, binds and bundles F-actin via its microtubule binding domain. *Curr. Biol.* **14,** 363–371 CrossRef Medline
49. Caceres, A., Payne, M. R., Binder, L. I., and Steward, O. (1983) Immunocytochemical localization of actin and microtubule-associated protein MAP2 in dendritic spines. *Proc. Natl. Acad. Sci. U.S.A.* **80,** 1738–1742 CrossRef Medline
50. Gong, C. X., Wegiel, J., Lidsky, T., Zuck, L., Avila, J., Wisniewski, H. M., Grundke-Iqbal, I., and Iqbal, K. (2000) Regulation of phosphorylation of neuronal microtubule-associated proteins MAP1b and MAP2 by protein phosphatase-2A and -2B in rat brain. *Brain Res.* **853,** 299–309 CrossRef Medline
51. Fan, Q. W., Yu, W., Senda, T., Yanagisawa, K., and Michikawa, M. (2001) Cholesterol-dependent modulation of tau phosphorylation in cultured neurons. *J. Neurochem.* **76,** 391–400 CrossRef Medline
52. Hotulainen, P., and Hoogenraad, C. C. (2010) Actin in dendritic spines: connecting dynamics to function. *J. Cell Biol.* **189,** 619–629 CrossRef Medline
53. Spence, E. F., and Soderling, S. H. (2015) Actin out: regulation of the synaptic cytoskeleton. *J. Biol. Chem.* **290,** 28613–28622 CrossRef Medline
54. Kilian, P., Campbell, S., Bilodeau, L., Guimond, M.-O., Roberge, C., Gallo-Payet, N., and Payet, M. D. (2008) Angiotensin II type 2 receptor stimulation increases the rate of NG108–15 cell migration via actin depolymerization. *Endocrinology* **149,** 2923–2933 CrossRef Medline
55. Okamoto, K., Nagai, T., Miyawaki, A., and Hayashi, Y. (2004) Rapid and persistent modulation of actin dynamics regulates postsynaptic reorganization underlying bidirectional plasticity. *Nat. Neurosci.* **7,** 1104–1112 CrossRef Medline
56. Dickey, A. S., and Strack, S. (2011) PKA/AKAP1 and PP2A/Bβ2 regulate neuronal morphogenesis via Drp1 phosphorylation and mitochondrial bioenergetics. *J. Neurosci.* **31,** 15716–15726 CrossRef Medline
57. Hoffman, P. N., and Lasek, R. J. (1975) The slow component of axonal transport: identification of major structural polypeptides of the axon and their generality among mammalian neurons. *J. Cell Biol.* **66,** 351–366 CrossRef Medline
58. Hoffman, P. N., Cleveland, D. W., Griffin, J. W., Landes, P. W., Cowan, N. J., and Price, D. L. (1987) Neurofilament gene expression: a major determinant of axonal caliber. *Proc. Natl. Acad. Sci. U.S.A.* **84,** 3472–3476 CrossRef Medline
59. Khazaei, M. R., Bunk, E. C., Hillje, A. L., Jahn, H. M., Riegler, E. M., Knoblich, J. A., Young, P., and Schwamborn, J. C. (2011) The E3-ubiquitin ligase TRIM2 regulates neuronal polarization. *J. Neurochem.* **117,** 29–37 CrossRef Medline
60. Hommel, J. D., Sears, R. M., Georgescu, D., Simmons, D. L., and DiLeone, R. J. (2003) Local gene knockdown in the brain using viral-mediated RNA interference. *Nat. Med.* **9,** 1539–1544 CrossRef Medline
61. Jiang, M., and Chen, G. (2006) High Ca^{2+}-phosphate transfection efficiency in low-density neuronal cultures. *Nat. Protoc.* **1,** 695–700 CrossRef Medline